JOURNAL OF NEUROTRAUMA 34:2154–2166 (July 1, 2017)

DOI: 10.1089/neu.2016.4744

A Three-Dimensional Computational Human Head Model That Captures Live Human Brain Dynamics

Shailesh Ganpule,[1] Nitin P. Daphalapurkar,[1] Kaliat T. Ramesh,[1] Andrew K. Knutsen,[2] Dzung L. Pham,[2] Philip V. Bayly,[3] and Jerry L. Prince[4]

Abstract

Diffuse axonal injury (DAI) is a debilitating consequence of traumatic brain injury (TBI) attributed to abnormal stretching of axons caused by blunt head trauma or acceleration of the head. We developed an anatomically accurate, subject-specific, three-dimensional (3D) computational model of the human brain, and used it to study the dynamic deformations in the substructures of the brain when the head is subjected to rotational accelerations. The computational head models use anatomy and morphology of the white matter fibers obtained using MRI. Subject-specific full-field shearing motions in live human brains obtained through a recently developed tagged MRI imaging technique are then used to validate the models by comparing the measured and predicted heterogeneous dynamic mechanical response of the brain. These results are used to elucidate the dynamics of local shearing deformations in the brain substructures caused by rotational acceleration of the head. Our work demonstrates that the rotational dynamics of the brain has a timescale of ~ 100 ms as determined by the shearing wave speeds, and thus the injuries associated with rotational accelerations likely occur over these time scales. After subject-specific validation using the live human subject data, a representative subject-specific head model is used to simulate a real life scenario that resulted in a concussive injury. Results suggest that regions of the brain, in the form of a toroid, encompassing the white matter, the cortical gray matter, and outer parts of the limbic system have a higher susceptibility to injury under axial rotations of the head.

Keywords: computational head model; DAI; human brain deformation

Introduction

Traumatic brain injury (TBI) is a critical public health problem worldwide with an estimated 10,000,000 people affected annually.[1] Global data indicate that nearly 60% of TBI occurrences are the result of road traffic accidents; ~20–30% are the result of falls; 10% are caused by violence, and another 10% are the result of sports and combat operations.[1] The rate of TBI incidence continues to grow with the increased adoption of motorized vehicles in developing countries, the faster pace of sports, and asymmetric military conflicts around the world. According to the World Health Organization, TBI will likely be the main cause of death and disability by the year 2020.[1]

Deformation of the brain tissue in response to a traumatic impact or rapid head acceleration can lead to numerous mechanical and chemical changes within the tissue. For example, during a concussion, rapid tissue strain is thought to cause diffuse depolarization of neurons.[2] In more severe trauma, diffuse axonal injury (DAI) can occur within the white matter of the brain, perhaps as a result of axonal stretch beyond a physiological injury threshold.[3] Animal models and *in vitro* mechanical testing support the hypothesis that abnormal tissue deformation is a fundamental cause of most brain injuries.[4] However, the susceptibility to injury of specific regions within the brain remains largely unknown.[5] Because injury-causing experiments cannot be performed on humans, human brain deformation dynamics leading to TBI have remained the subject of much speculation.[5]

Computational simulations can provide insights into the mechanics of abnormal deformations,[6,7] substituting for experiments that either cannot be performed for ethical reasons (e.g., injury-level accelerations in humans) or that are extremely difficult or expensive.[4,5] Biofidelic computer models[8–11] are invaluable tools for simulating dynamic deformations in the brain during an impact or head acceleration. Simulations can provide multi-scale descriptions of relevant mechanical variables such as strain and stress, given the physical properties of the human head and specific input

[1]Hopkins Extreme Materials Institute, Johns Hopkins University, Baltimore, Maryland.
[2]Center for Neuroscience and Regenerative Medicine, The Henry M. Jackson Foundation for the Advancement of Military Medicine, Bethesda, Maryland.
[3]Department of Mechanical Engineering, Washington University in St. Louis, St. Louis, Missouri.
[4]Department of Electrical and Computer Engineering, Johns Hopkins University, Baltimore, Maryland.

loading conditions (e.g., skull acceleration[12,13]). This capability is even more important for accident reconstruction, because it is not possible to measure the deformations in the living human brain during an actual injury event. Knowledge of the local deformation levels in the human brain is the first step toward being able to identify likely regions of injury in the brain.

Rotational accelerations are potentially more harmful than linear accelerations in DAI.[7,14,15] Despite advancements in sensing and measurement technology, accurate measurement of rotational accelerations during head trauma remains a nontrivial aspect even for laboratory experiments. Like many soft tissues, the brain is much more compliant under shear loads compared with volume-changing loads (e.g., pressure). This has two consequences. First, larger deformations are sustained in shear, so the substructures of the brain may be more prone to injury under shear. Second, and perhaps more important, the wave speeds associated with shearing deformations are at least an order of magnitude lower than that associated with volumetric deformations, resulting in a scale separation that can cause shear-driven injuries to occur at times much longer than those associated with pressure. This influence of the dynamics means that approaches designed to protect under pressure loads may not provide protection under shear loads (such as those resulting from rotational accelerations). Consequently, protection approaches and protocols must be designed to deal with a wider range of time scales and length scales than is commonly done today.

However, the question of how the rotational accelerations of the head might lead to injury remains largely unexplored.[7] Here, we examine the consequences of rotational accelerations on live human brains using computational simulations of subject-specific human heads in six subjects, and demonstrate the new capability to accurately capture the dynamics of shearing deformation in the live human brain. We developed three-dimensional (3D) virtual human head models (Fig. 1) using detailed MRI information for each subject, and incorporated subject-specific morphology of white matter fiber tracts into this high-structural-fidelity digital head through the use of diffusion tensor imaging (DTI). Models captured the anisotropic constitutive response of white matter fiber structure obtained from the DTI. Using subject-specific ''digital'' head models, we show that the computations have the ability to track the evolution of deformation in critical substructures of the living human brain. We focus on shearing deformations, as this remains a poorly understood yet critical realm in brain injury biomechanics.[3,14,16] Each subject-specific head model is quantitatively compared against full-field, time-varying measurements of displacements and shear strains[16,17] in subject-specific live human brains as described by Knutsen and coworkers.[18] To our knowledge, such a comparison of measured full-field deformation histories in the live human brain with the computational simulations has never been performed before. We obtained substantial insight even from the process of validation under such conditions. After subject-specific validation using the live human subject data, a representative subject-specific head model was used to simulate a real life scenario that produces a concussive injury. The ability of the model to provide insights into the degree and likely locations of injury is demonstrated for such an injury-causing event.

Our modeling approach is substantially different from finite element models of brain mechanical response in the literature[6–9,11] in two particular ways. First, our modeling approach is subject specific. We do not build a generic head model; rather, we build an individualized model for each subject, based on direct MRI imaging of the subject's anatomical and fiber tract orientation data; which include eight different anatomical structures (white matter, gray matter, caudate, putamen, thalamus, ventricles, cerebrospinal fluid [CSF], and subarachnoidal space [SAS]) for each individual subject. The subject-specific nature of the model allows us to ensure that the experimental validation corresponds to the subject-specific computational model, rather than the traditional case in which the computational model is based on a generic head that does

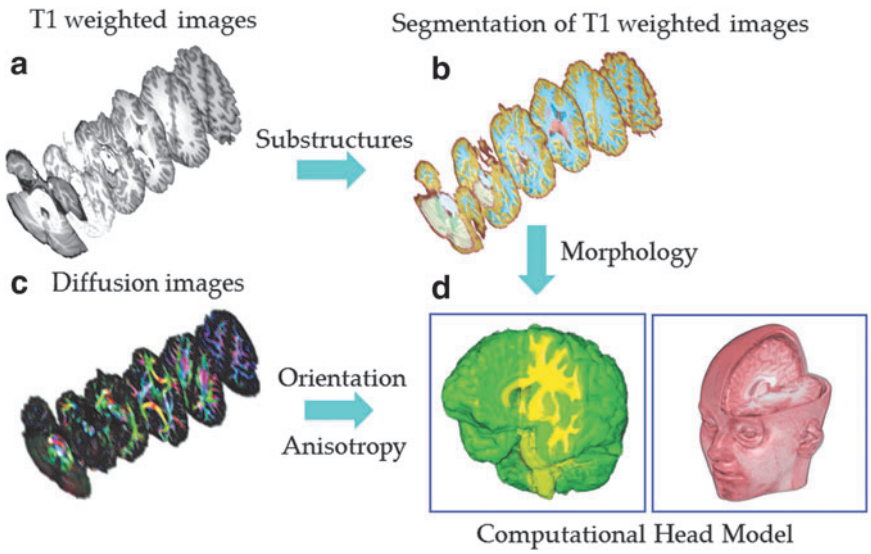

FIG. 1. The subject-specific, three-dimensional (3D) computational head model is created from T1-weighted MR images **(a)**. T1-weighted MR images are segmented into eight different substructures **(b)** by thresholding to the region of greatest probability for each pixel. These substructures are white matter, gray matter, caudate, putamen, thalamus, ventricles, cerebrospinal fluid (CSF), and subarachnoidal space (SAS). In addition to these substructures, the skull (not shown) is created by dilation of each MR slice by a number of pixels. Subject-specific fiber orientation and fractional anisotropy of the white matter is also incorporated in the subject-specific head model from diffusion imaging **(c)**. The resulting 3D head model **(d)** is digitized and kinematics under various loadings are solved using the material point method. Color image is available online at www.liebertpub.com/neu

not have the specific anatomical details associated with the experimental data set. Our validation approach is, therefore, much more constrained. Finally, the use of subject-specific models allows us to address the heterogeneity and variability of mTBI across the presenting population, which is not handled by any generic head model. Second, our modeling approach is based on the material point method (MPM),[19–21] rather than the finite element method (FEM). The material point method itself is not new; however, to our knowledge, it has never been utilized to study the dynamics of the human brain. The major improvements that we attain as a result of using the material point method are the following: 1) we are able to directly import voxelated information from MRI imaging of each subject to develop a computational model for each subject, so that there is little cost associated with developing a separate head model for each subject (this latter cost is huge for finite element models); 2) the material point method does not suffer from the excessive distortion limits developed in finite element models during large rotations of the type we discuss here, and, therefore, convergence questions can be explicitly addressed; 3) we are able to handle the very large ratio between the bulk modulus and the shear modulus of the brain tissue explicitly without volumetric locking artifacts (the ratio in our simulations, and in the brain, is 10^6).We also note that current advanced finite element (FE) codes can handle large differences in bulk and shear moduli without this issue.

Methods

In vivo *experiments on human subjects*

Experiments to obtain brain motion were conducted with the help of healthy human subjects recruited by the Center for Neuroscience and Regenerative Medicine (CNRM). This study was approved by the CNRM Institutional Review Board (IRB) at the National Institutes of Health. All subjects provided written informed consent prior to participation in the study. The experimental setup consisted of a head rotation device equipped to deliver a controlled angular acceleration onto a subject's head in an axial plane (i.e., rotation about an inferior-superior axis, see video S1) (see online supplementary material at http://www.liebertpub.com). Dynamic motions of subject-specific brains, under mild angular accelerations, were captured using an established quantitative imaging technique called tagged MRI.[16,17] Deformation measures, specifically, components of displacement vector and strain tensor, were computed from tagged MRI images using the harmonic phase (HARP) method.[17] As such, experimental data were obtained in 3D. However, the calculation of strain was restricted to two-dimensional (2D) (i.e., in-plane) strain components because of technical challenges associated with accurately calculating out-of-plane motion from the tagged images. Further, experiments were designed such that the head was subjected to pure rotational acceleration about a single axis. This simplified loading in the experiments has the advantage of primarily inducing 2D kinematics (i.e., significant in-plane motion and minimal out-of-plane motion) within the 3D head. Hence, in this article, we have focused on motions in a 2D plane only. Details on the experimental method have been provided elsewhere.[18]

Subject-specific digital head model

The subject-specific head model was built for total six human subjects (volunteers) (age range: 18–30 years). The head model considers the subject-specific anatomy of the brain. MRI (T1-weighted) images are segmented into different substructures using a topology-preserving, atlas-based technique.[22] The segmented structures are identified in Figure 1, and include white matter, gray matter, caudate, putamen, thalamus, ventricles, CSF, and SAS. Image processing (dilation of a brain mask) is used to generate an approximate, artificial ''skull.'' The segmented stack of images are exported in the form of voxelated data with a uniform spatial resolution of $2\times2\times2\,\mathrm{mm}^3$. These data, which carry with them subject-specific anatomy of the brain, are imported to the subject-specific head model with each voxel now representing a physical material volume. Contiguous material volumes are used to represent the structure of the brain (assumed as a continuum solid). The deformation response of the brain is computed with the help of a numerical method, called the material point method, to solve governing equations of motion, supplemented with initial conditions, boundary conditions, and material constitutive response. We used the UINTAH material point method package (uintah.utah.edu) to perform high-performance simulations on a computing cluster.

Constitutive models

The white matter of the brain consists of an organized morphology of fibers (bundle of axons) and the gray matter contains the cell bodies of neurons. The white matter tissue is generally considered anisotropic and the gray matter tissue is considered isotropic. A constitutive model, as applicable to an individual material volume, is an analytic model that relates a stress measure to a deformation measure, with the fidelity to consider the underlying fibrous morphology of the tissue. A number of previous studies[7,9,10] have found that the anisotropy of white matter (because of preferential fiber orientations) is critical for prediction of axonal strain and subsequent locations of injury. We modeled the white matter using the Holzapfel–Gasser–Ogden (HGO) strain energy function.[7,23] All other substructures were modeled using an isotropic limit of the HGO model. The constitutive model even incorporates the time-dependent response using a quasilinear viscoelastic function.[24] In this work, because viscous time constants are much larger than the simulation time, the contribution of viscous terms was minimal (if any). Details on the implementation of the constitutive model are available in Wright and coworkers.[7] The CSF was modeled as a fluid using the Tait equation of state,[25] given as

$$P=\frac{K_0}{n}\left[\left(\frac{\rho}{\rho_0}\right)^n-1\right]$$

where P is the pressure, K is the bulk modulus, and ρ is the density. The subscript '0' indicates values at zero pressure. For fluids similar in composition and viscosity to that of water, the value of constant $n=7.15$.[25] In addition, Newtonian behavior is assumed for shear.

Value for bulk modulus of the brain tissue used in computational head models varies significantly (by three orders of magnitude [for details and relevant references see Ganpule and coworkers[6]]) and remains uncertain because of lack of measurements in the literature. The dynamic bulk moduli of cerebrum ($K=1.46\,\mathrm{GPa}$) and cerebellum ($K=1.19\,\mathrm{GPa}$), were measured by one of the co-authors (K.T.R.) at high strain rates ($550\,\mathrm{s}^{-1}$ to $2700\,\mathrm{s}^{-1}$) using the compression Kolsky bar testing[26] on tissue samples from a postmortem human subject. The dynamic bulk modulus value is close to some other values (e.g., 2.1 GPa[27,28]) that are widely used in the literature.[8,29–32] Several material constants in the constitutive model are adopted from nanoindentation measurements available in the literature.[33] The anisotropic properties of the white matter tissue are calibrated[7] from data on tensile tests.[34] A comprehensive list of material properties and values are listed in Table 1.[25,33–36]

Incorporation of white matter anisotropy through DTI

In this work, axonal tracts were deformed based on the anisotropic constitutive response and they were not merely mapped against the deformation field. The fiber alignment vector a, and the degree of fiber dispersion, κ, are required inputs to the constitutive

TABLE 1. MATERIAL PROPERTIES OF HEAD CONSTITUENTS

Substructure	*Properties*	*Reference*
White matter	$G_0 = 1520$ Pa; $G_\infty = 286$ Pa; $g_1 = 0.81$; $\tau_1 = 2$ sec $k_1 = 121$ Pa; $k_2 = 0.0001$; fractional anisotropy (κ) and fiber direction ($\boldsymbol{a}$, unit vector) for each material point from diffusion tensor imaging (DTI)	33,34
Gray matter	$G_0 = 2750$ Pa; $G_\infty = 385$ Pa; $g_1 = 0.625$; $g_2 = 0.055$; $g_3 = 0.182$; $\tau_1 = 2$ sec; $\tau_2 = 11$ sec; $\tau_3 = 47.5$ sec	33
Caudate, putamen	$G_0 = 700$ Pa; $G_\infty = 110$ Pa; $g_1 = 0.61$; $g_2 = 0.135$; $g_3 = 0.103$; $\tau_1 = 1.45$ sec; $\tau_2 = 10$ sec; $\tau_3 = 110$ sec	33
Thalamus	$G_0 = 6700$ Pa; $G_\infty = 943$ Pa; $g_1 = 0.81$; $\tau_1 = 2$ sec	33
Common properties for brain substructures	$\rho = 1040$ kg/m^3; $K_{cerebrum} = 1.46$ GPa; $K_{cerebellum} = 1.19$ GPa	
Subarachnoid space (SAS)	$\rho = 1133$ kg/m^3; $E = 9.85$ MPa; $\upsilon = 0.45$	36
Skull	$\rho = 2070$ kg/m^3; $E = 8$ GPa; $\upsilon = 0.22$	35
Ventricles, cerebrospinal fluid (CSF)	$\rho = 1004$ kg/m^3; $K = 1.46$ GPa; $n = 7.15$; $\mu = 1.002$e-3 Pa-sec	25

model. These parameters vary spatially within the white matter of the brain and can be estimated from the DTI.[37] DTI is an MRI technique that provides an *in vivo* method for determining the orientation and anisotropy of white matter. The subject-specific DTI data were co-registered with subject-specific MRI images. The fiber alignment vector and the degree of fiber dispersion were estimated for individual voxels of the white matter.[37] Details of incorporation of white matter anisotropy through constitutive model and DTI are available elsewhere.[7] In brief, constitutive model used in this work (i.e., HGO strain energy function) took the following form:

$$W = \underbrace{\frac{\mu}{2}\left(\bar{I}_1 - 3\right) + \frac{k_1}{2k_2}\sum_{\alpha=1}^{N}\left\{e^{k_2\langle\bar{E}_\alpha\rangle^2} - 1\right\}}_{shear} + \underbrace{\frac{K}{2}\left(\frac{J^2-1}{2} - \ln J\right)}_{volumetric}$$

with

$$\bar{E}_\alpha = \kappa(\bar{I}_1 - 3) + (1 - 3\kappa)(\bar{I}_{4\alpha} - 1)$$

where, μ is the shear modulus of the isotropic matrix, k_1 is the stiffness of the fibers, k_2 is the dimensionless material parameter that controls the nonlinearity of the anisotropic response, N is the total number of fiber families (in the current work it was assumed that only a single family of fibers existed in the material; therefore, N was set equal to 1), K is the effective bulk modulus of the material, J is the volume change ratio, and κ is the structural parameter that defines the degree of fiber dispersion. The modified invariant, $\bar{I}_1$ and $\bar{I}_4$, are defined as

$$\bar{I}_1 = tr\left(\overline{\boldsymbol{C}}\right)$$

$$\bar{I}_4 = \boldsymbol{a^0} \cdot \overline{\boldsymbol{C}} \cdot \boldsymbol{a^0}$$

where, $\overline{\boldsymbol{C}}$ is the deviatoric component of the right Cauchy–Green deformation tensor and $\boldsymbol{a^0}$ is a unit vector representing the fiber direction in the reference configuration. Fiber direction can be obtained from DTI. When the material undergoes deformation, the vector $\boldsymbol{a^0}$ will deform with the body. After deformation, the fiber direction may be described by a unit vector $\boldsymbol{a}$. In general, the fibers will also undergo length change. The fiber stretch, λ, can be determined in terms of the deformation gradient and the fiber direction in the undeformed configuration:

$$\lambda \boldsymbol{a} = \boldsymbol{F} \cdot \boldsymbol{a^0}$$

because $\boldsymbol{a}$ is a unit vector:

$$\lambda^2 a \cdot a = \lambda^2 = \boldsymbol{a^0} \cdot \boldsymbol{F^T F} \cdot \boldsymbol{a^0} = \boldsymbol{a^0} \cdot \boldsymbol{C} \cdot \boldsymbol{a^0} = \bar{I}_4$$

The fiber orientation map and fractional anisotropy (FA) map from DTI provides the primary direction of fiber alignment and the degree of fiber dispersion respectively, for each voxel. Although the local fiber orientations can be directly obtained from the fiber orientation map, the fiber dispersion values determined from the FA map are not equal to the fiber dispersion parameter (κ) used in the HGO model. Fiber dispersion parameter κ can be related to FA from DTI using a relation (derived in Wright and coworkers[7]):

$$\kappa = \frac{1}{2}\frac{-6 + 4FA^2 + 2\sqrt{3FA^2 - 2FA^4}}{-9 + 6FA^2}$$

the lower limit of κ becomes 0, which represents regions with perfectly aligned fibers (i.e., transverse isotropy), and the upper limit becomes 1/3, which describes regions with randomly oriented fibers (i.e., isotropy).

Loading and boundary conditions

In the experiments,[18] a mild angular head deceleration in a human subject is generated after being initiated by voluntarily releasing a latch and coming to a rigid stop within a head support device. During the experiment, angular position histories are measured on the head rotation device in real-time using an MRI-compatible angular position sensor. Angular velocity and deceleration histories are computed from the recorded angular positions. The experimentally measured initial angular velocity and angular deceleration of the head act as initial conditions and boundary conditions to the head model, respectively. The head has an initial angular velocity of $\omega_0 = \sim 3.5$ rad/sec at $t = 0$ ms, after which it decelerates according to the angular deceleration history shown in Figure 2.

Method of solution

The material point method[19–21] is used to obtain dynamic analysis of the head model subjected to aforementioned loading conditions. In this numerical technique, the material volumes (also referred to as the material points) are used to represent a discretized material continuum. A background grid is used for solving governing equations (balance of linear momentum and balance of mass) and to determine spatial gradients using interpolation shape functions. The background grid does not deform. The material points are convected under the action of boundary conditions and are consistent with the materials constitutive response. The material point method has been applied to analyze a wide range of dynamic problems in solid mechanics and biomechanics, including dynamic material failure,[20,38] cellular mechanics,[39] and analysis of the ballistic impact on soft tissues and subsequent soft tissue failure.[40] In finite element modeling, element geometry typically corresponds to either hexahedral or tetrahedral elements. In the

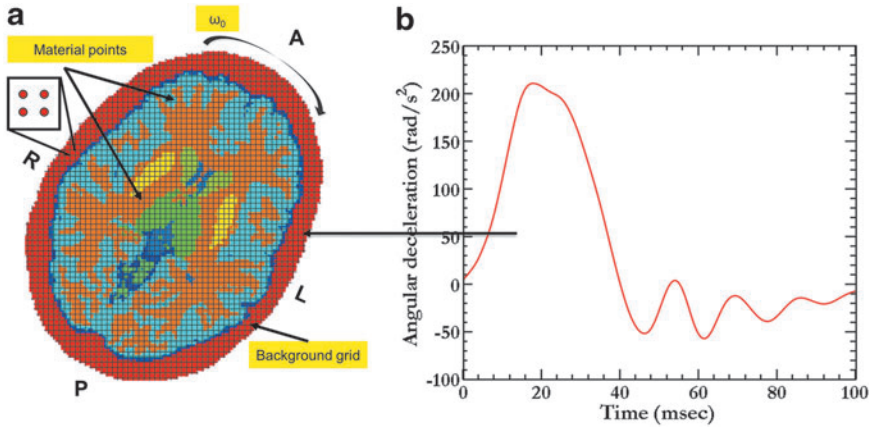

FIG. 2. The head models use a particle-based numerical method, the material point method (MPM), for dynamic analysis of a subject-specific human brain undergoing rotational acceleration. **(a)** shows a mid-axial section of the head model. Digitized image data from MRI images and diffusion tensor imaging (DTI) images were imported to the head model. A constant angular velocity, ω_0, acts as an initial condition for the head, as shown in **(a)**. Subsequently, the skull decelerates according to deceleration history shown in **(b)**. Both ω_0 and angular deceleration are based on the experimental measurements. Color image is available online at www.liebertpub.com/neu

MPM, becauses explicit meshing is not required, elements are only used for the background grid. The background grid is made up of hexahedral elements.

The MPM has several limitations. MPM is more computationally expensive than the FEM, as the field variables have to be interpolated from the particles to the grid and vice versa, and as the grid has to be reinitialized at the beginning of the new step. Energy dissipation error can occur in the MPM. Advanced techniques such as a time-stepping algorithm for stress calculation[41,42] and convected particle domain interpolation technique are required for alleviating the error.[21] Simulations in our article utilized the aforementioned techniques[21,41,42] to alleviate the energy dissipation.

Comparison of simulation predicted full-field data with tagged MRI measurements

Over the past few decades, the (bio) mechanics community has seen a tremendous rise in the use of computational models. The practice of using numerical models to design, build, and evaluate the performance of systems at the intersection of engineering and biology is gaining traction. Often, such models are validated at discrete spatial points because of the limitation in experimental measurements. One important aspect of the model development process—full spatial field model validation—has, however, received little attention. The evaluation of model validity becomes extremely critical when predictive capability is desired, especially to predict injuries, under dynamic loading conditions that typically result in spatially heterogeneous deformations. We propose a few statistical measures[43–46] to evaluate model validity. These measures are summarized in Table 2. Variables P and O represent a spatially varying simulated (predicted) data set and an experimentally measured (observed) data set, respectively. An overbar ($\overline{O}$) denotes the mean of the data set. Although there are uncertainties in the measured data, we assume that the measured data (O) is the ground truth for comparison of simulated results. A higher value of one of these statistical measures indicates a better agreement between simulated and measured data sets, except for the root mean square error (RMSE) observations standard deviation ratio (RSR) measure, for which a lower value indicates a better agreement. For some of the statistical measures described here (e.g. RSR, correlation score [CS]), the validity rating (or performance of a predictive model) in terms of a qualitative index (such as excellent, unacceptable) are adopted from the literature.[44,45] We use these ratings to indicate the agreement of simulated results with the measurements (Table 3).

Simulations of injurious loading

Rowson and coworkers[47] studied the rotational kinematics of the head associated with concussive impacts, using a head acceleration

TABLE 2. STATISTICAL MEASURES FOR EVALUATION OF FULL FIELD DATA BETWEEN THE MODEL AND THE EXPERIMENT

Statistical measure	*Equation*	*Range*	*Reference*
Index of agreement (d_r)	$d_r = \begin{cases} 1 - \frac{\sum_{i=1}^{N}\lvert O_i - P_i\rvert}{2\sum_{i=1}^{N}\lvert O_i - \overline{O}\rvert} \ \text{if} \ \lvert O_i - P_i\rvert \le 2\sum_{i=1}^{N}\lvert O_i - \overline{O}\rvert \\ \frac{\sum_{i=1}^{N}\lvert O_i - P_i\rvert}{2\sum_{i=1}^{N}\lvert O_i - \overline{O}\rvert} - 1 \ \text{if} \ \lvert O_i - P_i\rvert > 2\sum_{i=1}^{N}\lvert O_i - \overline{O}\rvert \end{cases}$	(–1) to 1	46
Coefficient of efficiency (E_2)	$E_2 = 1 - \frac{\sum_{i=1}^{N}\lvert O_i - P_i\rvert^2}{\sum_{i=1}^{N}\lvert O_i - \overline{O}\rvert^2}$	$-\infty$ to 1	43
Root mean square error (RMSE)-observations standard deviation ratio (RSR)	$RSR = \frac{RMSE}{STDEV_{obs}} = \frac{\sqrt{\sum_{i=1}^{N}(O_i - P_i)^2}}{\sqrt{\sum_{i=1}^{N}(O_i - \overline{O})^2}}$	0 to ∞	45
Correlation scores (CS)	$CS = (1 - \lvert NISE\rvert) \times 100 \ NISE = 1 - \frac{2\sum_{i=1}^{N} O_i P_i}{\sum_{i=1}^{N} O_i^2 + \sum_{i=1}^{N} P_i^2}$	0 to 100	44

NISE, normalized integral square error.

TABLE 3. MODEL PERFORMANCE EVALUATION STATISTICS

	Axial slice location	d_r	E_2	*RSR*	*CS*
Radial-circumferential shear strain (E_{rt})	Z = 40	0.48	–0.08	1.06 (unsatisfactory[a])	84.70 (good[a])
	Z = 20	0.55	0.02	0.99 (unsatisfactory[a])	91.20 (excellent[a])
	Z = 0	0.49	–0.07	1.04 (unsatisfactory[a])	86.19 (excellent[a])
	Z = –20	0.43	–0.12	1.09 (unsatisfactory[a])	78.90 (good[a])

[a]Validity rating (or performance of a predictive model).
RSR, Root mean square error (RMSE) observations standard deviation ratio; CS, correlation score.

data set collected in 335 collegiate football players. They report injury thresholds for various impact scenarios that resulted in definitive concussive injury. The impact scenarios are classified into three broad categories based on the direction of rotation as: impacts that result primarily in rotations in the sagittal plane, impacts that result primarily in rotations in the coronal plane, and the impacts that result primarily in rotations in the axial plane. We simulated the scenario that resulted primarily in rotation about the axial plane, as this closely resembles the loading simulated in the noninjurious case. This mode is dominated by significant rotational accelerations about the inferior-superior axis; that is α_z; with sagittal (α_x) and coronal (α_y) being negligible components (as recorded by the helmet sensors). Rowson and coworkers[47] report peak angular acceleration of 2192 rad/sec^2 as an injury threshold for the impacts that result in preliminary rotation about the axial plane. This peak acceleration value is used together with a representative acceleration pulse from Rowson and coworkers[12] as the loading input to the simulations (Fig. 6) . This peak acceleration value is an order of magnitude higher than the peak value used in the noninjurious loading case ($\sim$200 rad/sec^2) associated with the live human experiments. Also, the duration of the acceleration pulse is 18 ms for the injurious loading scenario as opposed to 40 ms for the noninjurious loading scenario.

Injury criterion

Our current understanding of the best injury criterion for DAI under rotational accelerations is that injury occurs[7] when the axonal tensile strains (rather than shear strains) reach a critical value.[48,49] The closest approximation to the axonal strains is provided by the axial strains along the fiber directions in the white matter fiber tracts. Because our head model includes the fiber orientations and our constitutive model[7] includes the anisotropic response because of underlying fiber tracts, we can compute the axial strains along the white matter fiber tracts. We use an axonal strain injury (ASI) criterion[7,10] to identify regions of the brain that exceed the ASI during the injurious loading scenario. We use two injury threshold values, a value of 18% defined by Wright and coworkers,[7] based on work of Bain and Meaney,[49] and a value of 13% defined by Giordano and Kleiven,[10] based on the work of Newman and coworkers.[50] Bain and Meaney[49] defined an optimal axonal strain threshold of 18% for the onset of electrophysiological impairment (a functional injury). Giordano and Kleiven[10] defined a white matter axonal threshold of 13% based on finite element calculations of accidental reconstructions[50] from the American National Football League (NFL). Strain rates for injurious loading simulated here and used while deriving ASI criteria are comparable. Strain rate for simulated injurious loading is $\sim$50 s^{-1}. Strain rate for ASI criteria of Wright and coworkers is $\sim$30–60 s^{-1}, whereas strain rate for ASI criteria of Giordano and Kleiven is $\sim$100–400 s^{-1}.

Quantification of injury

To quantify overall injury (damage) in white matter substructures, white matter tracts are further classified into three broad functional categories.[51] These categories are: 1) projection fibers (cortex–spinal cord, cortex-brainstem, and cortex–thalamus connections), 2) association fibers (cortex–cortex connections, limbic system tracts), and 3) callosal fibers (right–left hemispheric connections). We kept white matter tract segmentation to three broad categories for ease of interpretation of overall damage.

Results

Rotational dynamics of the live human brain

We performed 3D computational simulations of subject-specific human heads to study the dynamics of the shear wave propagation during a sudden deceleration (Fig. 3). During sudden deceleration of the head, the skull decelerates almost instantaneously, while the motion of the brain lags behind the motion of the skull. This lag in motion causes the brain to deform dynamically during deceleration

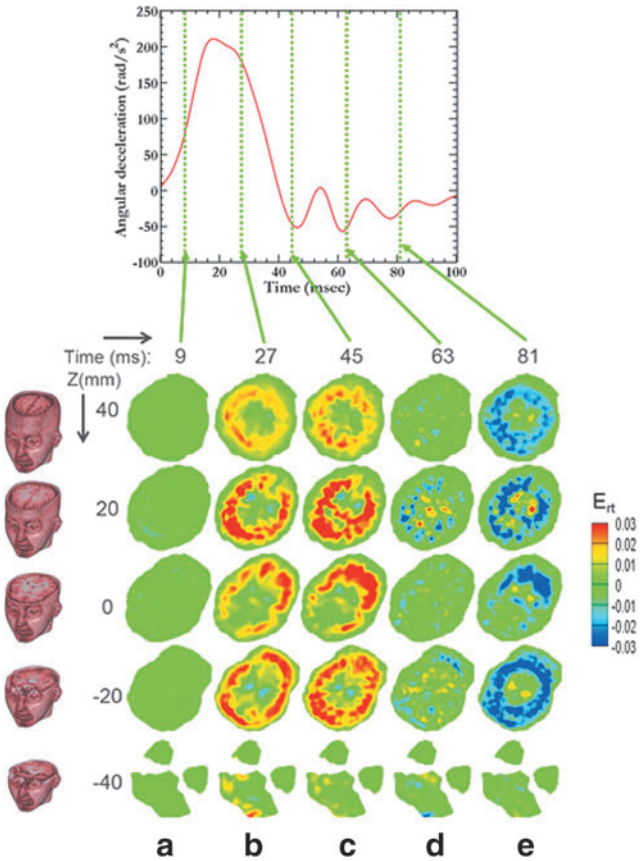

FIG. 3. Dynamics of wave propagation (simulated) in a human brain subjected to axial plane rotation. Radial-circumferential shear strain (E_{rt}) is used to illustrate wave propagation. Color image is available online at www.liebertpub.com/neu

(see Video S1). One manifestation of this motion is a shear wave propagating toward the center of the brain, as we demonstrate.

The wave propagation in the brain as a result of the sudden deceleration is illustrated in Figure 3 in terms of the computed radial-circumferential shear strain (E_{rt}), where the rows represent axial slices of the head and the columns represent the computed strain field in each slice at increasing times after deceleration begins. The rows are ordered top to bottom and are sections taken at various values of z, where the z axis is the inferior-superior axis of the human head, and the origin represents the centroid. The times presented correspond to times when experimental information is available (the corresponding accelerations are shown at the top of the figure), but the simulations include all intervening times. The figure shows that as the head decelerates, a shearing wave propagates from the exterior boundary toward the center (columns a–c). The wave propagation is truly 3D even for simulated quasi-2D motion of the head, and the interactions of the wave with the 3D structure of the brain are clearly visible in the individual slices. The propagation speed for the initial wave traversal is $\sim$1.2 m/sec, close to the elastic shear wave speed. As time proceeds, the shearing wave reflects from the center of the head and propagates back outward. The subsequent strain fields consist of a combination of reflected waves from the center traveling toward the external boundary and release waves traveling from the exterior boundary toward the center (as the deceleration decreases). By $\sim$100 ms, the strains appear to have been relaxed, but the kinetic energies in the system are still non-zero. The viscous dissipations are minimal at this time, because the viscoelastic relaxation times (1.5–47 sec) of the various substructures of the brain are at least an order of magnitude larger than the simulation time.

Validation of model against full-field live human brain data

We validate subject-specific computational head models against subject-specific, full-field live human brain data[18] with a focus on the shearing strains[3,14,16] (oft-used intracranial pressure is a much less discriminating measure for computational models of the brain, because of the near-incompressibility of brain tissue). Experiments were performed with spatial and temporal resolutions of 8 mm and 18 ms, respectively,[18] and the measured spatial displacements were then interpolated to obtain a full-field deformation map for the entire head. This information was used to extract displacement and strain fields for specific slices of the head for comparison with simulations performed on the subject-specific head model with identical input accelerations. The comparisons for a representative subject are shown in Figure 4. The full experimental and simulation data sets are massive, and, therefore, we chose only a handful of specific slices (the midaxial slice $z=0$ mm and the slices at $z=20$, -20, and 40 mms) for a range of times ($t=27$,45, 63, 81, and 99 ms), dictated by the temporal resolution of the experiment) to provide the comparison. For each slice, we show the experimental results in the left half and the simulation results in the right half. Figure 4 shows qualitatively (quantitative comparisons et seq.) that the computational model is able to capture the approximate magnitudes and dynamics of the experimentally observed strain fields in the live human brain, providing the validation of subject-specific computational models against live human brain data. Figure 4 shows that in both experiments and the simulations, a shear wave starts to propagate from the outer boundary toward the inside. Peak shear occurs at 45 ms, and, as time proceeds, shearing in the other direction (sign change) starts because of the reflection of waves from the center. The agreement between the experiment and the simulation appears reasonable in terms of strain magnitudes and overall distribution of strains.

An example of a more quantitative comparison of the experimental and computational results is presented in Figure 5a for a specific slice at a specific time using the conventional area-fraction approach.[18] Such an approach compares the area-fraction ϕ of each slice that has strains (ε) within specified range m to n, with the area fraction being defined by

$$\phi_{m<\varepsilon\leq n} = \frac{\iint \varepsilon dxdy,\ for\ m < \varepsilon \leq n}{\iint dxdy}$$

In addition, peak positive and peak negative shear strain (E_{rt}) in each substructure (such as white matter, gray matter) are also compared (Fig. 5b). The comparison between experiment and simulation is fair in terms of distribution of strains and strain magnitudes. A similar agreement between experiment and simulation is seen for other subjects (Fig. S1) (see online supplementary material at http://www.liebertpub.com), which demonstrates the robustness of the model in terms of the ability to translate from one subject to another.

The area fraction-based comparison approach described integrates out the heterogeneity of the strain field distribution. A more robust way to compare full-field data between the model and the experiment is to use broader statistical measures for model evaluation. Here, we

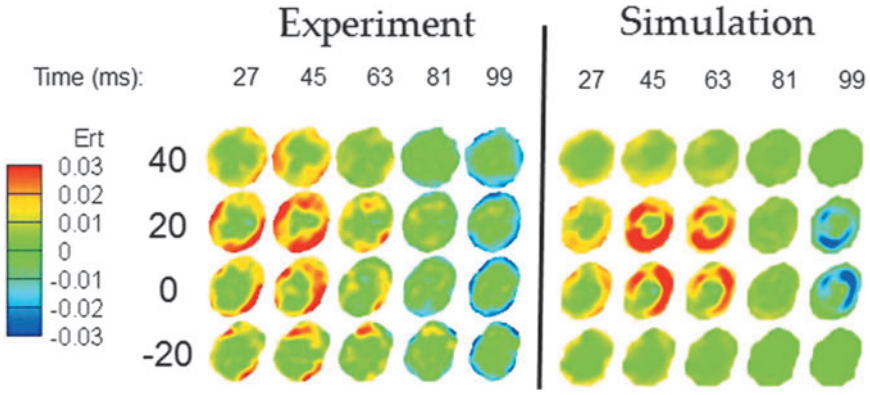

FIG. 4. Qualitative comparison of the radial-circumferential shear strain (E_{rt}) field between the experiment and the simulation. A representative result for a single subject is shown. Color image is available online at www.liebertpub.com/neu

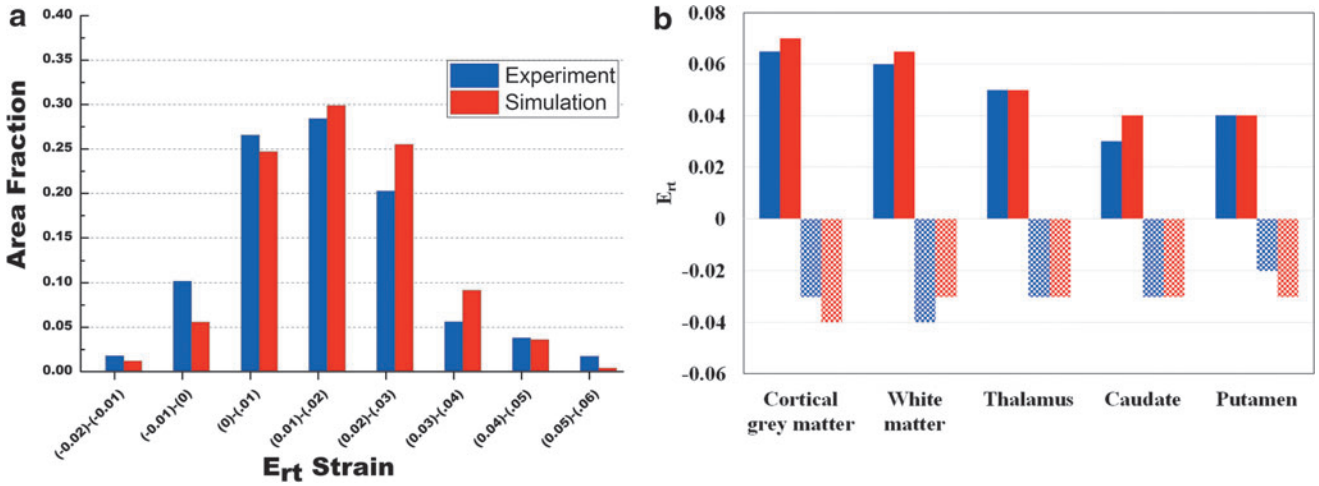

FIG. 5. **(a)** Quantitative comparison in terms of area fraction of th e radial-circumferential shear strain (E_{rt}) field between the experiment and the simulation. **(b)** Comparison of peak positive and peak negative radial-circumferential shear strain (E_{rt}) in each substructure. A representative result for a single subject is shown. Color image is available online at www.liebertpub.com/neu

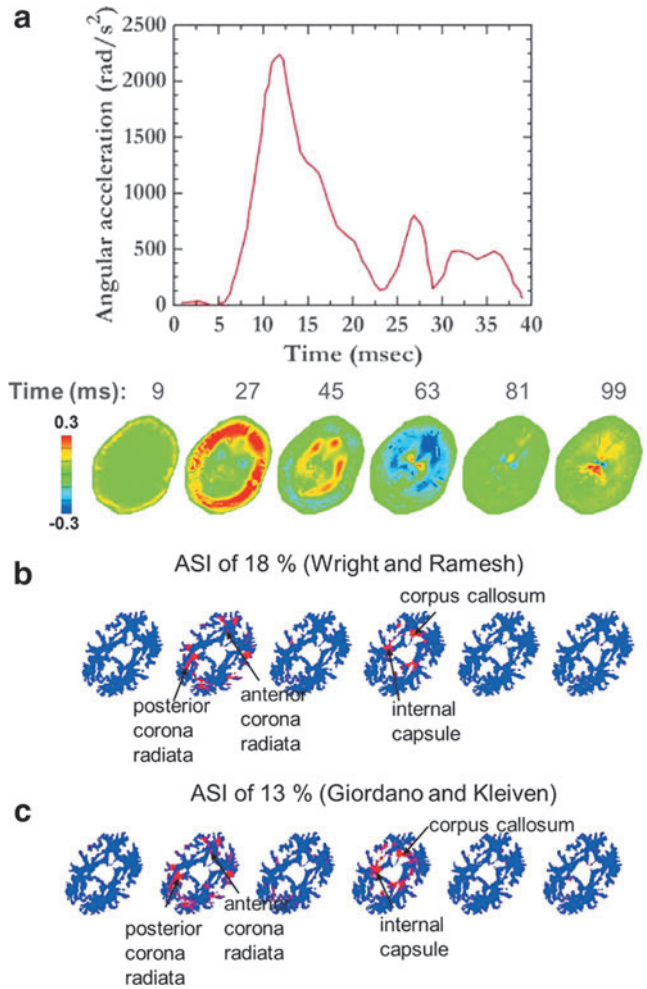

FIG. 6. **(a)** Input acceleration for injurious loading. **(b)** Radial-circumferential shear strain (E_{rt}) pattern in the brain for injurious loading. **(c)** Regions of white matter fiber tracts exceeding axonal strain injury (ASI) criterion. Injured (damaged) regions are marked in red. Color image is available online at www.liebertpub.com/neu

use a number of such measures (Table 2), mostly motivated from the climate community,[43–46] to estimate the degree of agreement between the model and the experiment. Table 3 shows the statistical evaluation of the model performance for a specific slice ($z=0$ mm), at a specific time ($t=45$ ms). Here, we evaluate the degree of model performance based on pointwise spatial variations at a fixed time. Conversely, the approach can be applied to evaluate temporal variations (in a given mechanical field) at a fixed point in space. Even though the qualitative agreement between the model and simulation (Fig. 4) appears reasonable, the quantitative comparison based on overall statistics at discrete spatial points is less definitive (Table 3). However, caution should be exercised while interpreting these results, as some of the validity ratings are based on the standards developed in the climate community, because of a lack of such standards in mechanics community. These measures are able to capture subtle differences between the model and the simulation, which are otherwise not apparent by visual comparison (Fig. 4). We note that although in general, comparison of temporal response at specific locations is an effective means to compare experiment and the simulation, in the current work, comparison of time histories between the experiment and the simulation is not useful, because of low temporal resolution (18 ms) in the experiments.

Sensitivity of the results to the material properties

To study the sensitivity of simulation results to material properties, particularly shear moduli, the baseline properties are scaled uniformly by ½, 2, and 4 times the original values. Figure S2 (see online supplementary material at http://www.liebertpub.com) shows the area fraction based distribution of radial-circumferential shear strain (E_{rt}) for various shear modulus values (for a representative subject); experimental strain distribution is also plotted. Because shear modulus values are different for each substructure, average (weighted by volume of each substructure) shear modulus is marked for each case. White matter and gray matter volumes comprise >95% of total volume, hence the average shear modulus is dominated by the values in white matter and gray matter. Further, these marked shear modulus values are closer to instantaneous shear modulus values, as relaxations times (sec) are much longer than the simulation time (ms), and hence viscous dissipation is

minimal. Based on the distribution of area fractions (Fig. S2), it is seen that the average shear modulus value of ~ 2.2 kPa gives the best agreement with the experimentally obtained response. Average shear modulus values of ~ 4.4 kPa and ~ 8.8 kPa produced a stiff response in which peak strains were underestimated, whereas shear modulus value of ~ 1.1 kPa produced a soft response in which peak strains were overestimated.

The global comparison approach based on area fraction integrates out the heterogeneity of the strain field distribution. Hence, an RMSE estimate that takes into account differences at each material point was also used for evaluating overall agreement between the experiment and the simulation. RMSE between the experiment and the simulation for various shear moduli are tabulated in Table S1(see online supplementary material at http://www.liebertpub.com). Based on RMSE estimates, a mean shear modulus value of ~ 2.2 kPa provides the least error (best agreement) with the experimentally obtained response. With shear modulus values of 2.2 ± 0.40 kPa, the RMSE error is <1%. As noted earlier, because viscoelastic time constants from low-rate experiments were used, viscous effects in the model were minimal, and this specific value of the shear modulus should be interpreted carefully.

Dynamic brain deformations during injury-causing loading

The validated head model presented previously is further used to simulate injurious loading that resulted in definitive concussion during collegiate football impacts. The specific head model used is a representative subject from the subjects examined in the noninjurious (validation) case. Figure 6 shows the strain evolution in the brain for injurious loading for a specific slice ($z = 0$ mm). The overall rotational dynamics (Fig. 6b) are similar to that observed in the noninjurious case. However, much larger shear strains are observed in this simulation, of the order of ±30%. Further, temporal variations in wave dynamics (e.g., time to peak experienced by various substructures) are also observed as compared with the noninjurious case, because of changes in the frequency of the loading pulse. Even with these spatiotemporal differences, overall time scale of the wave dynamics is 100 ms for injurious loading scenario, as limbic (innermost) regions of the brain experience the peak values at ~ 100 ms (Fig. 6b).

As stated earlier in the Methods section, we used ASI criteria to identify injured regions within the brain. We used the white matter ASI threshold values defined by Wright and coworkers[7] of 18% tensile strain and by Giordano and Kleiven[10] of 13% tensile strain. Using these injury thresholds, the specific white matter fiber tracts that would be injured (damaged), according to our simulations of this injurious loading scenario, are shown in Figure 6c. Notable damaged regions include the corpus callosum (with the highest damage of all tracts), cingulum, corona radiata, and internal capsule. Also, maximum damage occurs in the central portions of the brain as opposed to the cortical regions. This is because of the anisotropy of the brain tissue and preferential orientation of the fiber bundles along specific directions. Examining injury over the entire brain and for the entire simulation time of 100 ms, we can determine the degrees to which specific white matter substructures are likely to be injured in this scenario. Based on tract segmentation (for details refer to quantification of injury in the Methods section), we calculate injury (damage) in $\sim 10\%$ of projection fibers, $\sim 18\%$ of association fibers, and $\sim 22\%$ of callosal fibers over the entire brain and for the entire simulation time of 100 ms (Table 4). While quantifying the damage, once a given voxel is damaged it is not considered any further even if the injury threshold is exceeded at that voxel at later times.

Table 4. Damage Quantification in White Matter Fiber Tracts

	Cumulative damage (>100 ms)		
White matter substructure	*Axonal strain injury (ASI) (Wright and Ramesh)*	*ASI (Giordano and Kleiven)*	*Average of two injury threshold measures*
Projection fibers	9%	12%	10.5%
Association fibers	16%	20%	18%
Callosal fibers	21%	23%	22%

Discussion

In this work, we studied the dynamics of head rotation in live human volunteers subjected to mild (~ 200 rad/s^2) rotational acceleration. Our results indicate that the interaction of the rotational loading with the anatomical structure of the brain is seen to result in substantial heterogeneity (Fig. 3) in the strain pattern. Because some form of strain magnitude is often used[7] as an injury criterion, this indicates that the degree of injury will be spatially heterogeneous as well. The simulations and experiments (Figs. 3 and 4) also demonstrate that the rotational dynamics of the brain have a timescale of ~ 100 ms, as determined by the shearing wave speeds, and, therefore, the injuries associated with rotational accelerations are likely to occur over these time scales. This time scale may change slightly with better characterization of viscous time constants. Further, the time scales associated with the shearing information in the brain depend on both the material response (i.e., wave propagation speed in the material) and the frequencies in the loading pulse. Therefore, the entire range of times up to 100 ms may be important in these events. It is of note that even for injurious loading (Fig. 6), innermost limbic regions of the brain experience the peak values at ~ 100 ms, despite changes in the frequency of the loading pulse compared to noninjurious loading. This is important because much of the TBI mechanics literature (both experimental and computational) tends to focus on much smaller time scales.

The predictive capability of a computational head model can only be estimated after the model has been validated against available experimental data. As always, the key questions are 1) what experimental data set is used for validation, 2) is this experimental data set different from that used for calibration of the model, and 3) what is the degree of agreement between the simulation data set and the experimental data set. Ideally, the material and anatomical parameters that go into a head model should be obtained independently of the experimental data set used for validation. However, this is difficult, because there are few experimental data sets that can be used with the injury problem.

Most of the computational head models (see Yang and coworkers[52] and references therein) developed to study brain biomechanics are compared against measurements of intracranial pressures (made at a limited number of locations) in postmortem human subjects (PMHS). An interesting observation is that a very wide range (in terms of structural and material parameters) of computational head models can all replicate intracranial pressure

traces, and, therefore, this particular experimental data set is not able to discriminate between models. Therefore, although comparison of computed and measured intracranial pressures is valuable, this is not a sufficient validation of a computational head model. In addition to validation of intracranial pressure response, a few computational models of brain biomechanics have also been compared against[53,54] experimental measurements of brain displacement in PMHS.[8,10,11,29,32,55,56] These experiments and validation efforts are very encouraging, but are limited by the low spatial resolution of the displacement measurements (and therefore even poorer spatial resolution of the displacement gradients and hence the strains). Further, the geometry and anatomy of the head model are usually not the same as that of the head used in the experiment. Because of these challenges, there is currently no standard protocol for validation of computational biomechanics models of the head. Computational head models that claim ''validation'' can show differences of up to 100 % between experimentally measured and predicted responses.[8,10,11,29,32,55,56]

Here, considering the noninjurious case, we compare subject-specific head models against full-field deformation data measured noninvasively inside the living human brain of the identical living subject. This is the first comprehensive attempt toward comparing full-field deformation inside the brain tissue of a live human under prescribed loads. There is a one-to-one correspondence between the model and the experiment in morphology and fiber orientation of the brain tissue, loading conditions, and measured deformations. All of the model parameters are determined independently of the validation data set. For the comparisons, we focus on in-plane displacements and shearing strains for the reasons articulated in the Methods section of this article.

In spite of the conservative and rigorous approach we have used in the validation protocol (Figs. 4 and 5 and Table 3), the degree of agreement that we observe between the strains obtained in the experiments and predicted by the simulation is reasonable (Figs. 4 and 5) in terms of strain magnitudes and overall distribution of strains. Even though direct comparison cannot be made with other models,[8,10,11] the current acceptable standard in the literature for computational model validation appears to be differences on the order of ±100% when compared with experimental response. Full-field shearing deformations in the live human head have never been measured and used for validation before. Further, our simulations are able to match strain magnitudes, and strain distribution in each subject-specific head (Fig. S1). The error in magnitude of peak shear strain between simulations and experiments is $1.4 \pm 0.5\%$ for all the subjects. Another major difference between our approach and earlier validation efforts is that we compare full-field deformation fields as opposed to comparing at a limited number of discrete points inside the brain tissue. We believe that such a comprehensive approach toward validation will greatly enhance the predictive capabilities of the model, with implications in using computational head models for patient-specific diagnosis and care against DAI. We also propose statistical measures[43–46] (Table 2) for evaluation of model performance. Although a normalized integral square error (NISE) CS is generally used as a measure of model evaluation in the impact biomechanics community,[11,57] it tends to produce a relatively higher number (i.e., most liberal) compared with other model evaluation measures. Therefore, we believe that correlation score should not be used as an exclusive measure of model evaluation. It should be complemented with the other measures described in Table 2. The coefficient of efficiency (E_2) and RSR are difficult to interpret because of the lack of lower and upper bound, respectively, on these measures. In addition, these measures yield artificially higher values (toward ∞) if a deviation of O_i from the mean ($\overline{O}$) is small. On the other hand, index of agreement d_r is bounded by −1.0 and 1.0 and, in general, more rationally related to model accuracy than other model evaluation measures presented here. Index of agreement d_r is also quite flexible, making it applicable to a wide range of problems requiring model evaluation. Therefore, in addition to the conventional ''CS'' measure, we recommend ''index of agreement (d_r)'' as a potential measure for model evaluation. We emphasize that model evaluation measures as applied here are less definitive (Table 3) because of the lack of use of such measures in the (bio) mechanics community. We stress the utility of these methods for evaluation of model performance, with the hope that such a practice will bring out robust means for model evaluation in the (bio) mechanics community.

Comparison of full field strain fields between the experiments and the simulation (Fig. 4) also highlight some significant challenges. The comparison between simulation and experiment lacks agreement at times >45 ms (Fig. 4). This is likely because of the incomplete or inaccurate measurement of relevant viscoelastic time constants. It is also likely that the complex wave dynamics arising from the structural response are not captured properly by the simulations. Also, the experiments themselves have greater difficulty obtaining consistent data at very long times (as the subject's voluntary responses become engaged). The HGO strain energy function that we use does not account for the interaction between the white matter fibers and the effective matrix, and this might be important to fully represent a response of the brain tissue under dynamic loading. In addition, we did not explicitly model brain vasculature that can perhaps affect dampening, especially at later times.

After subject-specific validation in live human brains, we used a subject-specific head model (a representative subject) to predict the likely locations of injury in white matter fiber tracts under the injurious loading scenario. We used ASI threshold values[7,10] to identify regions of the brain that exceed the ASI during the injurious loading scenario. Based on these threshold values, our model predicted injury in the regions of the corona radiata, internal capsule, corticospinal tract, and corpus callosum (Fig. 6c) for axial rotation (i.e., rotation about an inferior-superior axis). The corona radiata, internal capsule, and corticospinal tract represent a motor pathway, and hence injury (damage) to these regions can presumably affect motor functions. The corpus callosum connects the right and left hemisphere and facilitates communication between the two sides of the brain. This neural tissue is also the largest collection of white matter within the brain, and contains a high myelin content which facilitates quicker transmission of information. Damage to the corpus callosum thus can lead to overall cognitive impairment. Microstructural changes in the corpus callosum are routinely observed among TBI populations in DTI imaging studies.[58] Quantification of injury based on tract-based segmentation (Table 4) suggests the highest damage to callosal fibers followed by association fibers and least damage to projection fibers. Such an approach can be extremely useful in a clinical setting to relate injury to functional outcomes, and also in establishing injury thresholds based on macroscopic (overall) damage to white matter as opposed to conventional head acceleration based thresholds.

The injured regions found in this work (corona radiata, internal capsule, corticospinal tract, and corpus callosum) are consistent with DTI findings in sports-related concussions. Meier and coworkers[59] collected DTI data in collegiate athletes (40 concussed, 46 control) at regular time intervals (1.64, 8.33, and 32.15 days)

post-concussion. They found changes in FA in longitudinal fasciculus, internal capsule, corona radiata, and corpus callosum with no evidence of recovery. Chamard and coworkers[60] conducted DTI studies in female athletes (8 concussed, 10 control) 6 months post-concussion. They particularly investigated two white matter regions, the corpus callosum and corticospinal tract, and found significant differences in the corpus callosum but no significant differences in the corticospinal tract in mean and radial diffusivities. Herweh and coworkers[61] conducted DTI studies in amateur boxers (31 concussed, 31 control). They found significant changes in FA and diffusivity measures in several white matter regions, including the corticospinal tract, internal capsule, corpus callosum, and longitudinal fascicle. Similar findings in injured white matter regions (albeit differences in quantitative trends) have been reported in other DTI studies[62–64] in TBI patients. The corpus callosum, internal capsule, and longitudinal fasciculus are commonly observed abnormal regions in these investigations. It should be noted that even though DTI studies are promising as a potential biomarker for mild TBI, the findings are still not robust in terms of quantifiable trends.

Limitations

In the current work, anisotropic material properties are based on the experiments of Velardi and coworkers[34] on porcine brain matter. Understanding the directional dependence of brain mechanical properties both *in vitro*[34,65–68] and *in vivo*[69] is still a topic of intense ongoing research, with varying results to date. Some studies of the corpus callosum in large mammals (lamb or sheep) found significantly stiffer response in the fiber direction than perpendicular to it.[34,66] On the other hand, another study of corpus callosum properties in the porcine brain found significantly stiffer response in shear perpendicular to the fiber than along the fiber.[65] In a recent investigation using postmortem human brain tissue, Budday and coworkers[68] found anisotropy of the brain tissue to be insignificant. Jin and coworkers,[67] on the other hand, found significant anisotropy in shear and minimal anisotropy in tension and compression in postmortem human brain tissue. Further, *in vitro* studies have shown that brain mechanical properties are affected by age[65,70] and loading mode.[68] Overall, additional investigations are likely needed to accurately account for mechanical anisotropy in white matter *in vivo*. As more reliable data become available, they should be incorporated in the computational modeling.

Viscous properties, including viscoelastic time constants used in this work, are taken from nanoindentation measurements on various substructures (e.g., white matter, caudate) of the brain. We chose these sets of properties because these appear to be the only measurements that provide the material response for individual anatomical regions (substructure) as opposed to the global properties that are typically used. The trade-off is that these measurements did not resolve high-strain rate behavior. In our experiments and simulations, the loading rates are $\sim 0.01\,s^{-1}$. At these rates, the effects of the modeled viscous terms in the simulation are minimal. However, better estimates of viscoelastic properties are likely needed to improve the agreement between simulation and experiments, especially at longer times (>45 ms).

Our model has not been systematically compared with high severity impacts. In addition to the comparison of model predictions to high-resolution strain fields *in vivo* described previously, a comparison of displacements predicted by the current head model was made to measurements of displacements of neutral-density markers in PMHS for higher severity impacts.[53,54] The goal of the current study is to capture live human brain dynamics, and it is well known that the material behavior[71,72] and internal boundary conditions[54] in PMHS are very different from those of live subjects. Hence, we believe, comparison of this model with the data obtained in PMHS is likely to be different and of limited value. However, for completeness, we briefly describe the comparison of model-predicted with to measured displacement data in PMHS.[53,54] The magnitude of displacements are similar to those reported for PMHS;[53,54] however, the frequency of displacement is not well captured (Fig. S3) (see online supplementary material at http://www.liebertpub.com). This mismatch can be attributed to several causes. 1) Because of limitations of the material point method and computational capacity, we cannot apply the very fast experimental loading and boundary conditions to the entire head. 2) At the very high levels of acceleration in the PMHS studies, the current model may not properly account for large deformation and high-rate viscoelastic behavior of the brain tissue. It is noteworthy that Gasser and coworkers[23] showed that for certain structural configurations (e.g., highly aligned fibers with nearly zero dispersion), the HGO model fails to accurately predict stiffening behavior at high stretches. We emphasize that although these limitations suggest that comparison of the experiment with simulation of brain motion *in vivo* at sub-injury levels is not *sufficient* to validate a model of brain injury at high rates, such a comparison is *necessary* to establish the ability to model basic biomechanics of the intact, living brain.

Conclusion

DAI, a type of TBI, has been strongly correlated to the rotational accelerations of the head. However, there is limited understanding of how rotational accelerations lead to DAI, which is normally attributed to abnormal stretching of axons. This work develops subject-specific computational head models that capture, for the first time, experimentally observed dynamics of brain deformations in live human subjects.

Full-field shearing deformations in the live human head have never been used for validation of models. Our work proposes statistical measures for evaluation of model performance. We recommend ''index of agreement (d_r)'' as a potential measure for model evaluation within the context of impact biomechanics, in addition to the commonly used conventional ''CS'' measure. Our simulations are able to match strain magnitudes and spatial distribution of strains in subject-specific brains.

Simulations using virtual head models allow for understanding of the mechanics associated with multi-scale dynamic deformations in the human brain. Our work demonstrates that, under elastic response, the rotational dynamics of the brain have a time scale of $\sim$100 ms as determined by the shearing wave speeds, and, therefore, the injuries associated with rotational accelerations likely occur over these timescales. By applying the model to a scenario that resulted in concussion, we demonstrate the ability to provide insights into the degree and likely locations of injury. Results suggest that susceptible regions of the brain, in the form of a toroid, encompassing the white matter, the cortical gray matter, and outer parts of the limbic system have a higher susceptibility to injury under axial rotations of the head.

Acknowledgments

S.G. acknowledges Dr. Fangxu Xing for useful discussions regarding the HARP algorithm, and Amy Dagro for assistance in proofreading the manuscript. The authors acknowledge funding from the National Institute of Neurological Disorders and Strokes,

National Institutes of Health (Project # R01NS055951). This work was partially supported by the Department of Defense in the Center for Neuroscience and Regenerative Medicine.

Author Disclosure Statement

No competing financial interests exist.

References

1. Hyder, A.A., Wunderlich, C.A., Puvanachandra, P., Gururaj, G., and Kobusingye, O.C. (2007). The impact of traumatic brain injuries: a global perspective. NeuroRehabilitation 22, 341–353.
2. Shaw, N.A. (2002). The neurophysiology of concussion. Prog. Neurobiol. 67, 281–344.
3. Graham, D., Adams, J.H., Nicoll, J., Maxwell, W., and Gennarelli, T. (1995). The nature, distribution and causes of traumatic brain injury. Brain Pathol. 5, 397–406.
4. Meaney, D.F., Morrison, B., and Bass, C.D. (2014). The mechanics of traumatic brain injury: a review of what we know and what we need to know for reducing its societal burden. J. Biomech. Eng. 136, 021008.
5. Bayly, P.V., Clayton, E.H., and Genin, G.M. (2012). Quantitative imaging methods for the development and validation of brain biomechanics models. Annu. Rev. Biomed. Eng. 14, 369.
6. Ganpule, S., Alai, A., Plougonven, E., and Chandra, N. (2013). Mechanics of blast loading on the head models in the study of traumatic brain injury using experimental and computational approaches. Biomech. Model. Mechanobiol. 12, 511–531.
7. Wright, R.M., Post, A., Hoshizaki, B., and Ramesh, K.T. (2013). A multiscale computational approach to estimating axonal damage under inertial loading of the head. J. Neurotrauma 30, 102–118.
8. Mao, H., Zhang, L., Jiang, B., Genthikatti, V.V., Jin, X., Zhu, F., Makwana, R., Gill, A., Jandir, G., and Singh, A. (2013). Development of a finite element human head model partially validated with thirty five experimental cases. J. Biomech. Eng. 135, 111002.
9. Giordano, C., Cloots, R., Van Dommelen, J., and Kleiven, S. (2014). The influence of anisotropy on brain injury prediction. J. Biomech. 47, 1052–1059.
10. Giordano, C., and Kleiven, S. (2014). Evaluation of axonal strain as a predictor for mild traumatic brain injuries using finite element modeling. Stapp Car Crash J. 58, 29.
11. Ji, S., Zhao, W., Ford, J.C., Beckwith, J.G., Bolander, R.P., Greenwald, R.M., Flashman, L.A., Paulsen, K.D., and McAllister, T.W. (2015). Group-wise evaluation and comparison of white matter fiber strain and maximum principal strain in sports-related concussion. J. Neurotrauma 32, 441–454.
12. Rowson, S., Beckwith, J.G., Chu, J.J., Leonard, D.S., Greenwald, R.M., and Duma, S.M. (2011). A six degree of freedom head acceleration measurement device for use in football. J. Appl. Biomech. 27, 8–14.
13. Hernandez, F., Wu, L.C., Yip, M.C., Laksari, K., Hoffman, A.R., Lopez, J.R., Grant, G.A., Kleiven, S., and Camarillo, D.B. (2015). Six degree-of-freedom measurements of human mild traumatic brain injury. Ann. Biomed. Eng. 43, 1918–1934.
14. Margulies, S.S., Thibault, L.E., and Gennarelli, T.A. (1990). Physical model simulations of brain injury in the primate. J. Biomech. 23, 823–836.
15. Ji, S., Zhao, W., Li, Z., and McAllister, T.W. (2014). Head impact accelerations for brain strain-related responses in contact sports: a model-based investigation. Biomech. Model. Mechanobiol. 13, 1121–1136.
16. Bayly, P., Cohen, T., Leister, E., Ajo, D., Leuthardt, E., and Genin, G. (2005). Deformation of the human brain induced by mild acceleration. J. Neurotrauma 22, 845–856.
17. Osman, N.F., McVeigh, E.R., and Prince, J.L. (2000). Imaging heart motion using harmonic phase MRI. IEEE Trans. Med. Imaging 19, 186–202.
18. Knutsen, A.K., Magrath, E., McEntee, J.E., Xing, F., Prince, J.L., Bayly, P.V., Butman, J.A., and Pham, D.L. (2014). Improved measurement of brain deformation during mild head acceleration using a novel tagged MRI sequence. J. Biomech. 47, 3475–3481.
19. Sulsky, D., Zhou, S.-J., and Schreyer, H.L. (1995). Application of a particle-in-cell method to solid mechanics. Comput. Phys. Commun. 87, 236–252.
20. Daphalapurkar, N., Hanan, J., Phelps, N., Bale, H., and Lu, H. (2008). Tomography and simulation of microstructure evolution of a closed-cell polymer foam in compression. Mech. Adv. Mat. Struct. 15, 594–611.
21. Sadeghirad, A., Brannon, R.M., and Burghardt, J. (2011). A convected particle domain interpolation technique to extend applicability of the material point method for problems involving massive deformations. Int. J. Numer. Methods Eng. 86, 1435–1456.
22. Bazin, P.-L., and Pham, D.L. (2008). Homeomorphic brain image segmentation with topological and statistical atlases. Med. Image Anal. 12, 616–625.
23. Gasser, T.C., Ogden, R.W., and Holzapfel, G.A. (2006). Hyperelastic modelling of arterial layers with distributed collagen fibre orientations. J. R. Soc. Interface 3, 15–35.
24. Fung, Y.-C. (2013). *Biomechanics: Mechanical Properties of Living Tissues.* Springer Science & Business Media, New York, NY.
25. Cole, R.H., and Weller, R. (1948). Underwater explosions. Phys.Today 1, 35.
26. Saraf, H., Ramesh, K., Lennon, A., Merkle, A., and Roberts, J. (2007). Mechanical properties of soft human tissues under dynamic loading. J. Biomech. 40, 1960–1967.
27. Stalnaker, R.L. (1969). Mechanical properties of the head [PhD dissertation]. West Virginia University, Morgantown.
28. McElhaney, J.H., Melvin, J.W., Roberts, V.L., and Portnoy, H.D. (1973). Dynamic characteristics of the tissues of the head, in: *Perspectives in Biomedical Engineering: Proceedings of a Symposium Organised in Association with the Biological Engineering Society and Held in the University of Strathclyde, Glasgow, June 1972*. R.M. Kenedi (ed.). Palgrave Macmillan UK: London, pps. 215–222.
29. Kleiven, S., and Hardy, W.N. (2002). Correlation of an FE model of the human head with local brain motion: Consequences for injury prediction. Stapp Car Crash J. 46, 123–144.
30. Horgan, T.J., and Gilchrist, M.D. (2004). Influence of FE model variability in predicting brain motion and intracranial pressure changes in head impact simulations. Int. J. Crashworthiness 9, 401–418.
31. Zhang, L., Yang, K.H., Dwarampudi, R., Omori, K., Li, T., Chang, K., Hardy, W.N., Khalil, T.B., and King, A.I. (2001). Recent advances in brain injury research: A new human head model development and validation. Stapp Car Crash J. 45, 369–394.
32. Zhang, L., Yang, K.H., and King, A.I. (2004). A proposed injury threshold for mild traumatic brain injury. J. Biomech. Eng. 126, 226–236.
33. Lee, S., King, M., Sun, J., Xie, H., Subhash, G., and Sarntinoranont, M. (2014). Measurement of viscoelastic properties in multiple anatomical regions of acute rat brain tissue slices. J. Mech. Behav. Biomed. Mater. 29, 213–224.
34. Velardi, F., Fraternali, F.. and Angelillo, M. (2006). Anisotropic constitutive equations and experimental tensile behavior of brain tissue. Biomech. Model. Mechanobiol. 5, 53–61.
35. McElhaney, J.H., Fogle, J.L., Melvin, J.W., Haynes, R.R., Roberts, V.L., and Alem, N.M. (1970). Mechanical properties of cranial bone. J. Biomech. 3, 495–511.
36. Jin, X., Lee, J.B., Leung, L.Y., Zhang, L., et al. (2006). Biomechanical response of the bovine pia-arachnoid complex to tensile loading at varying strain-rates. Stapp Car Crash J. 50, 637–649.
37. Pierpaoli, C., Walker, L., Irfanoglu, M., Barnett, A., Basser, P., Chang, L., Koay, C., Pajevic, S., Rohde, G., Sarlls, J., and Wu, M. (2010). TORTOISE: an integrated software package for processing of diffusion MRI data, in: *18th Scientific Meeting of the International Society for Magnetic Resonance in Medicine*, International Society for Magnetic Resonance in Medicine, Stockholm, Sweden, p. 1597.
38. Sulsky, D., and Schreyer, L. (2004). MPM simulation of dynamic material failure with a decohesion constitutive model. Eur. J. Mech. A Solids 23, 423–445.
39. Guilkey, J.E., Hoying, J.B., and Weiss, J.A. (2006). Computational modeling of multicellular constructs with the material point method. J. Biomech. 39, 2074–2086.
40. Ionescu, I., Guilkey, J.E., Berzins, M., Kirby, R.M., and Weiss, J.A. (2006). Simulation of soft tissue failure using the material point method. J. Biomech. Eng. 128, 917–924.
41. Bardenhagen, S. (2002). Energy conservation error in the material point method for solid mechanics. J. Comput. Phys. 180, 383–403.
42. Nairn, J.A. (2003). Material point method calculations with explicit cracks. Comp. Mod. Eng. Sci. 4, 649–664.
43. Legates, D.R., and McCabe, G.J. (1999). Evaluating the use of ''goodness-of-fit'' measures in hydrologic and hydroclimatic model validation. Water Resour. Res. 35, 233–241.
44. Kimpara, H., Nakahira, Y., Iwamoto, M., Miki, K., Ichihara, K., Kawano, S., and Taguchi, T. (2006). Investigation of anteroposterior

head-neck responses during severe frontal impacts using a brain-spinal cord complex FE model. Stapp Car Crash J. 50, 509–544.
45. Moriasi, D.N., Arnold, J.G., Van Liew, M.W., Bingner, R.L., Harmel, R.D., and Veith, T.L. (2007). Model evaluation guidelines for systematic quantification of accuracy in watershed simulations. Biol. Eng. Trans. 50, 885–900.
46. Willmott, C.J., Robeson, S.M., and Matsuura, K. (2012). A refined index of model performance. Int. J. Climatol. 32, 2088–2094.
47. Rowson, S., Duma, S.M., Beckwith, J.G., Chu, J.J., Greenwald, R.M., Crisco, J.J., Brolinson, G.P., Duhaime, A.-C., McAllister, T.W., and Maerlender, A.C. (2012). Rotational head kinematics in football impacts: an injury risk function for concussion. Ann. Biomed. Eng. 40, 1–13.
48. Gennarelli, T.A., Thibault, L.E., and Graham, D.I. (1998). Diffuse axonal injury: an important form of traumatic brain damage. Neuroscientist 4, 202–215.
49. Bain, A.C., and Meaney, D.F. (2000). Tissue-level thresholds for axonal damage in an experimental model of central nervous system white matter injury. J. Biomech. Eng. 122, 615–622.
50. Newman, J.A., Shewchenko, N., and Welbourne, E. (2000). A proposed new biomechanical head injury assessment function–the maximum power index. Stapp Car Crash J. 44, 215–247.
51. Wakana, S., Jiang, H., Nagae–Poetscher, L.M., van Zijl, P.C., and Mori, S. (2004). Fiber tract-based atlas of human white matter anatomy. Radiology 230, 77–87.
52. Yang, K.H., Mao, H., Wagner, C., Zhu, F., Chou, C.C., and King, A.I. (2011). Modeling of the brain for injury prevention, in: *Neural Tissue Biomechanics*. Springer, Berlin and Heidelberg, Germany, pps. 69–120.
53. Hardy, W., Foster, C., Mason, M., Yang, K., King, A., and Tashman, S. (2001). Investigation of head injury mechanisms using neutral density technology and high-speed biplanar X-ray. Stapp Car Crash J. 45, 337–368.
54. Hardy, W.N., Mason, M.J., Foster, C.D., Shah, C.S., Kopacz, J.M., Yang, K.H., King, A.I., Bishop, J., Bey, M., Anderst, W., and Tashman, S. (2007). A study of the response of the human cadaver head to impact. Stapp Car Crash J. 51, 17.
55. Takhounts, E.G., Ridella, S.A., Hasija, V., Tannous, R.E., Campbell, J.Q., Malone, D., Danelson, K., Stitzel, J., Rowson, S., and Duma, S. (2008). Investigation of traumatic brain injuries using the next generation of simulated injury monitor (SIMon) finite element head model. Stapp Car Crash J. 52, 1–31.
56. Sahoo, D., Deck, C., and Willinger, R. (2014). Development and validation of an advanced anisotropic visco-hyperelastic human brain FE model. J. Mech. Behav. Biomed. Mater. 33, 24–42.
57. Kimpara, H., Nakahira, Y., Iwamoto, M., and Miki, K. (2006). Investigation of anteroposterior head-neck responses during severe frontal impacts using a brain-spinal cord complex FE model. Stapp Car Crash J. 50, 509.
58. Hulkower, M.B., Poliak, D.B., Rosenbaum, S.B., Zimmerman, M.E., and Lipton, M.L. (2013). A decade of DTI in traumatic brain injury: 10 years and 100 articles later. AJNR Am. J. Neuroradiol. 34, 2064–2074.
59. Meier, T.B., Bergamino, M., Bellgowan, P.S., Teague, T.K., Ling, J.M., Jeromin, A., and Mayer, A.R. (2016). Longitudinal assessment of white matter abnormalities following sports-related concussion. Hum. Brain Mapp. 37, 833–845.
60. Chamard, E., Lefebvre, G., Lassonde, M., and Theoret, H. (2016). Long-term abnormalities in the corpus callosum of female concussed athletes. J. Neurotrauma 33, 1220–1226.
61. Herweh, C., Hess, K., Meyding–Lamadé, U., Bartsch, A.J., Stippich, C., Jost, J., Friedmann–Bette, B., Heiland, S., Bendszus, M., and Hähnel, S. (2016). Reduced white matter integrity in amateur boxers. Neuroradiology 58, 911–920.
62. Murugavel, M., Cubon, V., Putukian, M., Echemendia, R., Cabrera, J., Osherson, D., and Dettwiler, A. (2014). A longitudinal diffusion tensor imaging study assessing white matter fiber tracts after sports-related concussion. J. Neurotrauma 31, 1860–1871.
63. Gardner, A., Kay–Lambkin, F., Stanwell, P., Donnelly, J., Williams, W.H., Hiles, A., Schofield, P., Levi, C., and Jones, D.K. (2012). A systematic review of diffusion tensor imaging findings in sports-related concussion. J. Neurotrauma 29, 2521–2538.
64. Eierud, C., Craddock, R.C., Fletcher, S., Aulakh, M., King–Casas, B., Kuehl, D., and LaConte, S.M. (2014). Neuroimaging after mild traumatic brain injury: review and meta-analysis. NeuroImage Clin. 4, 283–294.
65. Prange, M.T., and Margulies, S.S. (2002). Regional, directional, and age-dependent properties of the brain undergoing large deformation. J. Biomech. Eng. 124, 244–252.
66. Feng, Y., Okamoto, R.J., Namani, R., Genin, G.M., and Bayly, P.V. (2013). Measurements of mechanical anisotropy in brain tissue and implications for transversely isotropic material models of white matter. J. Mech. Behav. Biomed. Mater. 23, 117–132.
67. Jin, X., Zhu, F., Mao, H., Shen, M., and Yang, K.H. (2013). A comprehensive experimental study on material properties of human brain tissue. J. Biomech. 46, 2795–2801.
68. Budday, S., Sommer, G., Birkl, C., Langkammer, C., Haybäck, J., Kohnert, J., Bauer, M., Paulsen, F., Steinmann, P., and Kuhl, E. (2017). Mechanical characterization of human brain tissue. Acta Biomater. 48, 319–340.
69. Romano, A., Scheel, M., Hirsch, S., Braun, J., and Sack, I. (2012). In vivo waveguide elastography of white matter tracts in the human brain. Magn. Reson. Med. 68, 1410–1422.
70. Gefen, A., Gefen, N., Zhu, Q.L., Raghupathi, R., and Margulies, S.S. (2003). Age-dependent changes in material properties of the brain and braincase of the rat. J. Neurotrauma 20, 1163–1177.
71. Garo, A., Hrapko, M., Van Dommelen, J., and Peters, G. (2007). Towards a reliable characterisation of the mechanical behaviour of brain tissue: the effects of post-mortem time and sample preparation. Biorheology 44, 51–58.
72. Chatelin, S., Constantinesco, A. and Willinger, R. (2010). Fifty years of brain tissue mechanical testing: from in vitro to in vivo investigations. Biorheology 47, 255–276.

Address correspondence to:
Shailesh Ganpule, PhD
Hopkins Extreme Materials Institute
Johns Hopkins University
Baltimore, MD 21218

E-mail: sganpul1@jhu.edu